Unveiling Trajectories: Breakthroughs in Muon Tracking for CONNIE Experiment

1st Santiago Ferreyra
Facultad de Ingeniería
Universidad Nacional de Asunción
San Lorenzo, Paraguay
sferreyra@fiuna.edu.py

2nd Oscar Baez
Facultad de Ingeniería
Universidad Nacional de Asunción
San Lorenzo, Paraguay
oscarbaez@fiuna.edu.py

3rd Diego Stalder
Facultad de Ingeniería
Universidad Nacional de Asunción
San Lorenzo, Paraguay
dstalder@ing.una.py

4th Jorge Molina
Facultad de Ingeniería
Universidad Nacional de Asunción
San Lorenzo, Paraguay
jmolina@ing.una.py

***Abstract*—This study introduces an innovative muon tracking algorithm designed for the Coherent Neutrino-Nucleus Interaction Experiment (CONNIE). In this experiment, a cluster of twelve charge-coupled device (CCD) sensors is strategically positioned in close proximity to the Angra II nuclear reactor. The primary objective of the experiment is the detection of antineutrinos produced by the reactor, serving as a gateway to investigating non-standard neutrino interactions through Coherent Neutrino-Nucleus Scattering (CEvNS). However, the images acquired by these sensors reveal an abundance of muonic particles, originating from the collision of cosmic rays with the Earth's atmosphere. This study is fundamentally focused on the advancement of a muon tracking system that will allow to trace the trajectories of the muons or any other particle with high energy. The GEANT4 toolkit has been used to create synthetic images that will be used to validate the algorithm, that will be use in the analysis of images collected by the CCDs of the experiment. In this work, we evaluated the algorithm's performance using synthetic images, achieving an efficiency of 98.78%. This result underscores the algorithm's robustness and reliability in reconstructing muon trajectories.**

***Index Terms*—CONNIE, muon, tracking**

I. Introduction

In the domain of particle physics experiments, achieving accurate reconstruction of particle trajectories—referred to as tracking—serves as a pivotal foundation for unraveling the essential characteristics of the subatomic realm. Exemplified by milestones like the TrackML, Higgs Boson, and Flavour of Physics challenges in machine learning for particle physics, the importance of tracing particle paths resonates [1], [2]. These challenges highlight the critical nature of tracking particle trajectories within detectors like the Large Hadron Collider (LHC) at CERN. As experiments like DUNE and ProtoDUNE push boundaries, there is an increased urgency for precise tracking to decode the intricate interactions occurring within particle detectors. This tracking process essentially pieces together the puzzle of particle behavior, unveiling the distinct signatures left behind by particles in experiments.

979-8-3503-6953-3/23/$31.00 ©2023 IEEE

Reconstructing trajectories fundamentally involves finding measurements (events) linked to the same particle when it passes thought the detector, posing a combinatorial challenge. Existing solutions are generally based on well-established tracking-based algorithms requires the identification of the new features to associate the events in different parts of the detectors. Pattern recognition and deep learning algorithms have been applied in various experiments, as noted by [1]. In this study, our aim is to identify trajectories and their associated metrics for particles navigating through the detectors of the CONNIE experiment.

The CONNIE experiment, centered on Coherent Neutrino-Nucleus Interaction, highlights the vital role of accurate tracking. It deploys 12 charge-coupled device sensors near the Angra II nuclear reactor located in Angra dos Reis, Brazil [3]. In this context, an algorithm is required to track muonic particles, originated from the collision of cosmic rays with the Earth's atmosphere. These particles are the main source of the background noise for the detection of neutrinos interactions coming from a nuclear reactor.

The images captured by CCD sensors in the CONNIE experiment encompass a variety of features, including electron-induced patterns (referred to as "worms"), distinct spots signifying alpha, gamma, or vertical muons, overlapped events, as well as regular muons. This diversity of particle signatures poses a challenge in discriminating among them. To address this, our pipeline has incorporated automated algorithms for classifying and instance segmenting these particles, as documented in [**?**]. However, effectively tracking muons across the 12 CCD sensors presents an intricate challenge due to the high event density caused by the 3-hour exposure time. Muons, being high-energy charged particles, generate distinctive patterns within detectors depending on the incidence angle. A robust tracking algorithm is essential for accurate identification and association of muon-induced features, especially the vertical ones, which appear as spots. Developing this algorithm requires establishing connections between signals detected by

different CCDs, a complex task given the complexity of muon interactions and the resulting patterns on individual CCDs. To address this complexity, simulations of muon interactions with CONNIE detectors can be carried out employing a toolkit designed for simulating particle passage through matter, such as GEANT4 [4] the muon interactions that were simulated with this program served to validate the efficacy of the tracking algorithm.

II. Dataset

The data used in the training process of the system are images obtained from simulations performed with the GEANT4 package. This software allows accurate simulation of the particles of interest (muons) with the atoms that compose the detector, Silicon in our case. In this context, the muons are simulated such that it is possible to capture and record the energy deposition at every step of their trajectory. This allows to correspond the coordinates the amount of energy recorded for each pixel, forming the images in the same way as the CCDs do.

The distribution used for launching the particles is the cosine-square function from the azimuth angle [5], like Fig. 1 shows. It can be seen that 10 detectors are aligned, maintaining a consistent spacing between them. This enables a muon to potentially interact with none, one, several, or all of the detectors depending on the angle of incidence. The three sets, namely Set 1, Set 2, and Set 3, consist of simulated muon events captured by the CCD sensors. Set 1 comprises 1480 unique impacts on the CCDs, Set 2 consists of 1445 unique impacts, and Set 3 encompasses 1462 unique impacts. Each impact corresponds to a registered event within the CCD sensors during the simulated experiment. These sets serve as distinct collections of data, capturing various scenarios of muon interactions and their resulting impacts on the detectors.

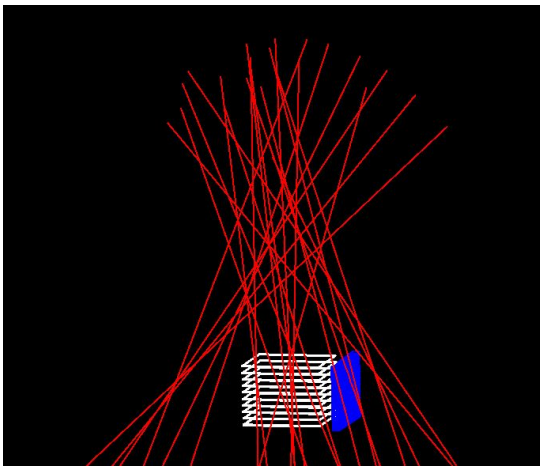

Fig. 1. Simulation of muons launched according to the cosine square of the azimuthal angle that will impact the detectors at different angles as in the real case.

III. Feature Engineering

In the realm of CCD sensor image analysis, referred to as frames, each frame commonly captures the impacts of numerous muons. The tracking algorithm is bifurcated into two stages: the initial stage predicts the position on the subsequent CCD, while the subsequent stage involves event association based on similarity metrics. Within this context, a critical phase involves the extraction of informative features from each impact, effectively represented as a digital image. These features establish a fundamental groundwork for comprehending particle dynamics within the sensor environment. This section elucidates the employed methodology for feature extraction, highlighting its pivotal role in unveiling the intricate dynamics of particles encapsulated within individual frames.

The features extracted from each impact encompass image size ($S = \{s_x, s_y\}$), the centroid ($C = \{c_x, c_y\}$), and the asymmetry of the impact ($A = \{a_x, a_y\}$). The image size characterizes the dimensions of the impact area. It is calculated as the range of x and y coordinates spanned by the hits:

$$s_x = \max(x_i) - \min(x_i), \quad s_y = \max(y_i) - \min(y_i), \quad (1)$$

where i are the hit positions along the x and y axes, respectively. The centroid is determined through the averaging of the positions associated with a specific impact on a given CCD. This value offers an estimation of the particle's impact location on the detector, and is computed as follows:

$$c_x = \frac{1}{N}\sum_{i=1}^{N} x_i, \quad c_y = \frac{1}{N}\sum_{i=1}^{N} y_i, \quad (2)$$

where i denote the hit positions of the muon on the CCD, and N represents the number of hits associated with each muon impact. While the asymmetry, it gauges how close or far the centroid is from the center of the window. This relationship is determined as follows with respect to the centroid:

$$a_x = c_x - \frac{1}{2}(x_{\text{max}} + x_{\text{min}}), \quad a_y = c_y - \frac{1}{2}(y_{\text{max}} + y_{\text{min}}), \quad (3)$$

the assessment of impact shape and distribution within the window, as well as the identification of entry angles, relies heavily on the concept of asymmetry.

Fig. 2 provides a visualization of the feature extraction process applied to a frame within each event image. By depicting the interplay of these extracted features, the figure sheds light on the intricate details that contribute to the understanding of particle interactions within the context of individual frames.

In order to establish a systematic organization of this data, these parameters are computed for each registered event in every CCD. These values are presented in the form of a table, establishing connections between the various parameters and each individual event, as well as the corresponding interacting CCD.

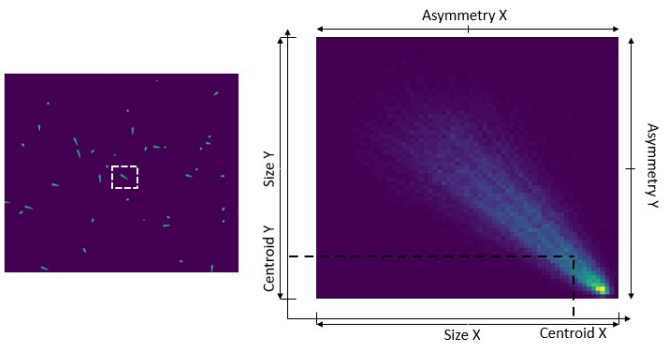

Fig. 2. Feature extraction of a frame for each impact, encompassing the identification of the event size, determination of centroid, and assessment of impact asymmetry.

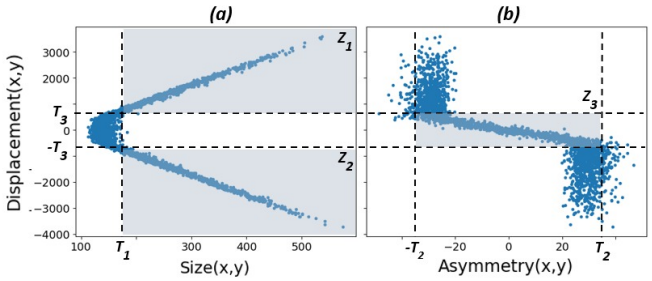

Fig. 3. Linearity observed between displacement, size and asymmetry.

IV. Tracking Algorithm

This section outlines the two distinct stages of the algorithm designed for accurate muon tracking within the CCD sensors. These stages are formulated to sequentially address key aspects of the tracking process. The first stage focuses on predicting the subsequent position of muon impacts, while the second stage pertains to the precise association of elements within a defined window size. Through this dual-stage approach, the algorithm aims to enhance the precision and reliability of muon trajectory reconstruction.

A. Stage A: Position Prediction through Linear Regression

This stage involves prediction the displacement (d_x, d_y) of the impact bounding box center between CCDs, taking into account the features extracted in the preceding section. As depicted in Fig. 3(a), the event size (s_x, s_y) exhibits a linear correlation with the displacement. However, it's noteworthy that this correlation becomes less reliable when the event size reaches 170 microns, at which point it introduces noise. To address this limitation, Fig. 3(b) demonstrates how asymmetry complements the information needed for events with a smaller displacement, exhibiting a linear correlation for such instances. By combining both features, we can establish a robust foundation for defining a new search region in the subsequent CCD.

To estimate the parameters of the linear regression (LR), we divide the regions of interest into three zones: Z_1, Z_2, and Z_3. The first two zones exhibit symmetry with respect to the axis of window size, as depicted in Fig. 3(a). On the other hand, the third zone is defined in terms of asymmetry, as shown in Fig. 3(b). These zones are determined by three thresholds: T_1, T_2, and T_3, which represent the criteria for window size, impact asymmetry, and particle displacement, respectively.

In the algorithm, events with displacements larger than the specified threshold (T_1) undergo evaluation through a linear regression (LR) based on the event size equation (4). Conversely, events with displacements smaller than T_1 are assessed based on their asymmetry using equation (5). The regression equations are defined as follows:

$$E_k = s_k \cdot m_{\text{size}} + b_{\text{size}}, \text{ when } T_1 \geq s_k \text{ para } k \in \{x, y\} \quad (4)$$

$$E_k = a_k \cdot m_{\text{asym}} + b_{\text{asym}}, \text{ when } T_1 < s_k \text{ para } k \in \{x, y\}, \quad (5)$$

here, E_x and E_y signify the estimated bounding box center in the subsequent CCD, while m_{size}, b_{size}, m_{asym}, and b_{asym} are parameters that have been estimated and calibrated. Finally, the position of the new bounding box relative to the initial CCD is determined considering an oblique incidence. Notably, the asymmetry provides a highly reliable indication of the event's direction, enabling us to accurately select the appropriate quadrant for locating the corresponding event on the subsequent CCD.

B. Stage B: Window-based Association

This stage comprises two distinct steps. The initial step entails defining a search window (W_1) to locate the potential impacts on the CCD, wherein multiple candidates may be situated (Fig. 4). Subsequently, the second step involves utilizing similarity metrics to discern and select the appropriate event from the candidates identified in the previous step (Fig, 5).

To initiate the search, start by selecting an event p, in a CCD_i, where $i \in 1, 2, ..., 10$, denoted by E^{p,CCD_i}. Utilize linear regression to determine the optimal alignment with the event parameters and forecast potential impact point coordinates in the subsequent CCD_{i+1}. Establish a bounding box around this point using W_1 and identify all suitable candidate events that are encompassed by it, as depicted in Fig. 4.

This initial step exhibits a variation when two events are matched in contiguous CCDs. In such cases, given the ability to trace a line between them, the search window can be reduced, denoted by (W_2). This reduction is possible because predicting the next position becomes more accurate in such scenarios, resulting in lower error. This decision is driven by the fact that having an event and its prediction substantially enhances the accuracy of estimating the displacement for the subsequent event.

During the second step, the candidates within the search window are subject to evaluation using comparison metrics to establish the event that bears the greatest similarity. When a prediction is pinpointed as the most favorable candidate, the discrepancy between this prediction and the event detected

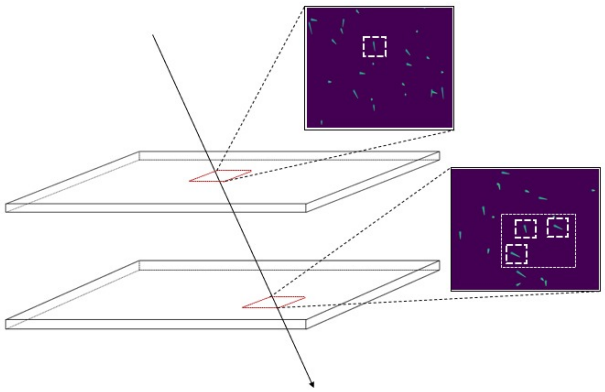

Fig. 4. Selection of an event and search for the best prediction among the candidates for the trajectory in the first search window (W_1).

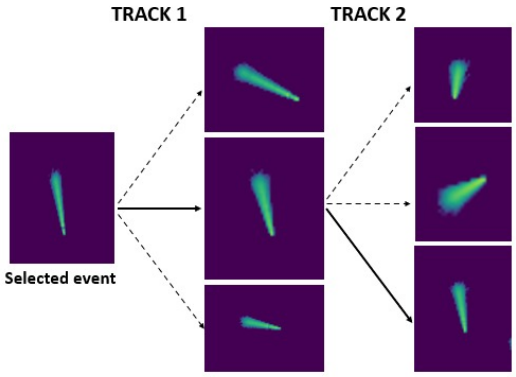

Fig. 5. Selection of an event and comparison with possible predictions in order to determine the trajectory.

in the preceding detector is calculated, as depicted in Fig. 5. This discrepancy serves as a guiding element for exploring the subsequent detector based on the parameters of the present prediction. This iterative procedure continues between a chosen event and the selected prediction until the ultimate possible impact along the trajectory is discerned.

To assess the similarity between the projected original event, denoted as $E^{p,CCD_{i+1}}$, and each candidate event (j) within the search window in CCD_{i+1}, the L2 norm is utilized. This metric measures the proximity between the feature vectors of the two events. The feature vector encompasses the event's size, centroid coordinates, and asymmetry values. The calculation of the L2 norm between $E^{p,CCD_{i+1}}$ and a candidate event $E^{j,CCD_{i+1}}$ is expressed as:

$$\text{Similarity}(E^{p,CCD_{i+1}}, E^{j,CCD_{i+1}}) = M_1 + M_2 + M_3 \quad (6)$$

where, $M_1 = |S^{p,CCDi+1} - S^{j,CCDi+1}|_2$, $M_2 = |C^{p,CCDi+1} - C^{j,CCDi+1}|_2$, $M_3 = |A^{p,CCDi+1} - A^{j,CCDi+1}|_2$.

The L2 norm $|\cdot|_2$ computes the squared Euclidean distance between these feature vectors, signifying their similarity for event association. By calculating the L2 norm for all candidate events, the algorithm identifies the event j with the highest similarity to event p, where the prediction with the highest similarity to the event is the one with the lowest numerical similarity value, as this is the L2 norm, the smaller distances imply higher accuracy, enabling precise event association.

Hence, within the event record, all impact points identified by the search linked to a specific event are assigned. Subsequently, the evaluation of a subsequent impact is undertaken, conducting searches among those that have not yet been assigned. Through this iterative process, all events are visited and associated with a specific event by the culmination of the procedure. The two stages are summarized in the Algorithm 1.

When examining synthetic data, each particle trajectory is known, allowing for accurate verification of all event associations. Consequently, our algorithm's assignments can be cross-checked against this known ground truth for correctness. Thus, the algorithm's "efficiency" can be defined as the ratio of correctly assigned impacts to the total number of impacts:

$$efficiency = 100 \cdot \left(\frac{\sum_{i=1}^{N} \text{events}[i = \text{hit}]}{M} \right), \quad (7)$$

equation 7 presents the mathematical definition of the efficiency metric utilized in the algorithm. Here, the events that are considered hits through the (N) detectors are evaluated against the number (M) of events recorded in their entirety.

Algorithm 1 Tracking algorithm

procedure STAGE A(Event E_i)
  Select an event E^{p,CCD_i} with features (S_i, C_i, A_i)
  Perform LR to estimate displacement $\{d_{x_i}, d_{y_i}\}$
  Calculate predicted position $E^{p,CCD_{i+1}} = (c_{x_i} + d_{x_i}, c_{y_i} + d_{y_i})$
  Create a search window around $E^{p,CCD_{i+1}}$ using W_1 or W_2.
  Identify candidate events j within the search window.
end procedure
procedure STAGE B(Event $E^{j,CCD_{i+1}}$)
  for each candidate event j in the search window **do**
    Calculate similarity metrics between $E^{p,CCD_{i+1}}$ and $E^{j,CCD_{i+1}}$
  end for
  Identify the candidate event with the highest similarity.
  Asociate the events and repeat the process for each CCD.
end procedure

V. Experimental results

This section presents a comprehensive analysis of the tracking algorithm's performance. Divided into multiple subsections, it covers aspects such as the impact of linear regression in Stage A prediction, optimization of window size and thresholds for Stage B, evaluation of efficiency on each CCD, and the

influence of data discretization. Through these analyses, the section provides valuable insights into the algorithm's effectiveness, accuracy, and adaptability across different scenarios and parameters.

A. Linear Regression for Stage A

Table I presents the outcomes of the linear regression procedure, furnishing parameter values obtained from the linear regression analysis for each dataset. The parameters m_{size} and b_{size} denote the slope and intercept, respectively, utilized for predicting event size. Similarly, m_{asym} and b_{asym} denote the slope and intercept for predicting asymmetry. The table exhibits computed values for each dataset, namely Set 1, Set 2, and Set 3, showing notable similarities. These consistent values hold the potential to be employed for estimating displacements, providing valuable insights into the algorithm's predictive capabilities.

Fig. 6 illustrates the fitted linear regression (LR) models employed in stage A for predicting positions on the subsequent CCD_{i+1}. To optimize threshold selection, we present an evaluation outlined in Table II. This table systematically explores various parameter sets to identify the combination that yields the highest efficiency. The highlighted row in the table denotes the configuration that resulted in the highest efficiency, reaching an impressive 98.92%. This achievement was made with the following threshold values: $T_1 = 172$, $|T_2| = 45$, and $|T_3| = 600$.

TABLE I
LINEAR REGRESSION

	m_{size}	b_{size}	m_{asym}	b_{asym}
$Set1$	7.690	-573.368	-15.404	-4.886
$Set2$	7.673	-570.319	-14.916	-4.695
$Set3$	7.680	-574.226	-15.545	-4.269
Average	7.681	-572.638	15.288	-4.616

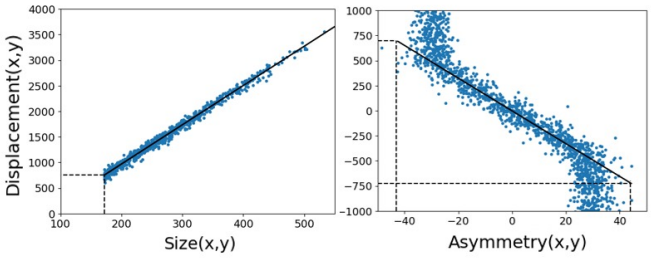

Fig. 6. Fitted Linear Regression (LR) models: Panel (a) depicts the relationship between displacements D_x and D_y as functions of event sizes S_x and S_y respectively; Panel (b) illustrates the relationship between D_x and D_y in relation to asymmetry parameters A_x and A_y.

Finally, we assessed the goodness of fit for both considered linear regressions using Pearson's correlation coefficient. This statistical test quantifies the linear relationship between two continuous variables and provides a coefficient that can vary from +1 to -1. A value of 0 signifies no correlation between the variables, while a positive or negative value indicates a positive or negative relationship. In our case, the Pearson's coefficient for the first adjustment exceeded 0.98, and for the second adjustment, it surpassed 0.94. This high coefficient indicates that both linear regression models provide a good fit to the data, reaffirming their accuracy in predicting the displacements.

TABLE II
COMBINATIONS OF THRESHOLDS AND EFFICIENCIES

T_1	T_2	T_3	Efficiency
169			97.50
172	25	300	97.567
175			97.229
	35		98.648
172	45	300	98.716
	55		98.716
		400	98.716
172	45	600	98.918
		800	98.716
172	45	600	98.918

B. Adjustment of windows size W_1, W_2

In order to optimize the window sizes for Stage B and achieve maximum efficiency, an additional experiment was conducted. Table III illustrates the evaluation of various sets in terms of the window size (W_1) of the initial bounding box. The efficiency of each set is reported, along with the count of misses, representing instances where events were not accurately associated. Similarly, Table IV presents the assessment of different sets with respect to the window size (W_2) of the subsequent bounding box. Once again, the efficiency of each set and the corresponding number of misses are provided. This iterative process aids in fine-tuning the algorithm by identifying the optimal window sizes, thereby enhancing its ability to predict and associate events across the CCD sensors with improved accuracy.

TABLE III
ASSESSMENT OF DIFFERENT SETS BASED ON THE WINDOW SIZE (W_1) OF THE FIRST BOUNDING BOX, SHOWCASING THE CORRESPONDING EFFICIENCY AND THE COUNT OF MISSES EVENTS

Set1	W_1						
	300	400	500	600	700	800	900
Efficiency	96.621	98.243	98.378	98.581	98.513	98.243	98.108
Misses	50	26	24	21	22	26	28

TABLE IV
ASSESSMENT OF DIFFERENT SETS BASED ON THE WINDOW SIZE (W_2) OF THE FIRST BOUNDING BOX, SHOWCASING THE CORRESPONDING EFFICIENCY AND THE COUNT OF MISSES EVENTS

Set1	W_2						
	50	100	150	200	250	300	350
Efficiency	93.175	96.554	98.243	98.513	98.581	98.581	98.243
Misses	101	51	26	22	21	21	26

C. Evaluation of efficiency of the calibrated algorithm

This subsection presents a detailed comparison between the event associations generated by the tracking algorithm and the corresponding real results from the simulation data. To achieve

this, we quantify the number of hits caused by muons passing through a variable number of CCDs, ranging from 10 to 1. This approach allows us to calculate the percentage of events that correctly match the algorithm using the ”efficiency”. This metric provides a quantitative measure of the algorithm's ability to accurately associate events for each CCD.

Fig. 7 effectively underscores the algorithm's exceptional efficiency in consistently and precisely associating impact events across a range of CCDs. The efficiencies observed, spanning from approximately 96% to a perfect 98%, underscore the algorithm's robust capability to forecast and match impact events with remarkable accuracy. The evaluation metric indeed underscores the high efficiency evident in the algorithm's adept prediction of impacts for the detectors.

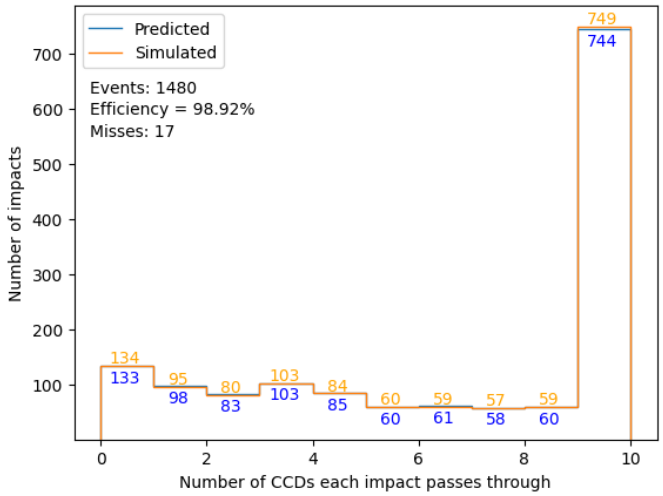

Fig. 7. Number of impacts for muons passing through different CCDs, highlighting differences between associated events and true simulated events corresponding to the most efficient algorithm.

In the context of this research, it is important to emphasize that all evaluations were performed using simulations. To carry out the case study, discretized images with a bin size of 15 microns per pixel were used. This choice of resolution is the one used in the experiment with synthetic images that realistically simulate the scenario in question.

The synthetic images used in these simulations yielded an efficiency of 98.78%. This value is significant because it indicates that no significant variation in the performance of the tracking method is observed when digitizing the data. These results strongly support the feasibility and robustness of the technique under real data conditions. The simulation results strongly support the applicability of the tracking method in practical settings, paving the way for its effective implementation in a variety of scientific and engineering applications.

VI. Conclusions

In conclusion, this study introduces an novel tracking algorithm that effectively addresses the challenge of associating impact events across multiple CCDs. By combining the strengths of linear regression-based predictions and similarity metrics, the proposed algorithm showcases remarkable accuracy and efficiency in event association. The two-stage framework, comprising position prediction and event matching, demonstrates its ability to handle diverse scenarios and varying impact event characteristics.

The calibration and optimization of window sizes and thresholds showcased in this study contribute to the algorithm's enhanced performance. The experimentally determined parameters not only fine-tune the algorithm's predictive capabilities but also establish a foundation for accurate event association. The evaluation of different datasets and algorithm features further highlights the reliability of the algorithm across various scenarios.

One of the significant achievements of this research is the outstanding efficiency of 98.78% achieved by the algorithm in accurately predicting and matching impact events, as demonstrated through extensive simulations. These consistently high efficiencies underscore the algorithm's potential for real data applications in particle detection. However, the transition from synthetic to real images taken in experiments introduces challenges such as background noise, interactions of other particles with the detectors, and potential misalignment during assembly of the CCDs. These aspects will be subjects of analysis in future collaborative efforts aimed at refining and adapting the algorithm for real-world applications and other experiments such as particle detection experiments such as [6].

Acknowledgment

Authors acknowledge the financial support given the Engineering Faculty (FIUNA) and the data provided by the CONNIE experiment. JM and DHS acknowledges the FEEI-PROCIENCIA-CONACYT-PRONII.

References

[1] M. Kiehn, S. Amrouche, P. Calafiura, V. Estrade, and S. Farrell, “The trackml high-energy physics tracking challenge on kaggle,” *EPJ Web of Conferences*, p. v, 2019.

[2] C. Adam-Bourdarios, G. Cowan, C. Germain-Renaud, I. Guyon, B. Kégl, and D. Rousseau, “The higgs machine learning challenge,” *Journal of Physics: Conference Series*, vol. 664, no. 7, p. 072015, dec 2015. [Online]. Available: https://dx.doi.org/10.1088/1742-6596/664/7/072015

[3] A. Aguilar-Arevalo, X. Bertou, C. Bonifazi, M. Butner, G. Cancelo, A. C. Vazquez, B. C. Vergara, C. Chavez, H. D. Motta, J. D'Olivo, J. D. Anjos, J. Estrada, G. F. Moroni, R. Ford, A. Foguel, K. P. H. Torres, F. Izraelevitch, A. Kavner, B. Kilminster, K. Kuk, H. Lima, M. Makler, J. Molina, G. Moreno-Granados, J. Moro, E. Paolini, M. S. Haro, J. Tiffenberg, F. Trillaud, and S. Wagner, “The connie experiment,” *Journal of Physics: Conference Series*, vol. 761, no. 1, p. 012057, oct 2016. [Online]. Available: https://dx.doi.org/10.1088/1742-6596/761/1/012057

[4] S. Agostinelli, J. Allison, K. Amako, and et al., “Geant4—a simulation toolkit,” *Nuclear Instruments and Methods in Physics Research Section A: Accelerators, Spectrometers, Detectors and Associated Equipment*, vol. 506, no. 3, pp. 250–303, 2003. [Online]. Available: https://www.sciencedirect.com/science/article/pii/S0168900203013688

[5] J. Bremer and F. Nobels, “Characterising the cosmic rays in a ccd,” *Kapteyn Astronomical Institute, Groningen*, 2015.

[6] A. Aguilar-Arevalo and et al., “The oscura experiment,” *TBD*, 2 2022. [Online]. Available: https://www.osti.gov/biblio/1854820